


Global study of the scalar quasinormal modes of Kerr-AdS₅ black holes: Stability, thermality, and horizon area quantization

Issei Koga,¹ Naritaka Oshita², and Kazushige Ueda¹

¹*Department of Physics, Kyushu University, 744 Motoooka, Nishi-Ku, Fukuoka 819-0395, Japan*

²*RIKEN iTHEMS, Wako, Saitama 351-0198, Japan*

 (Received 8 March 2022; accepted 31 May 2022; published 21 June 2022)

We numerically explore the structure of quasinormal (QN) frequencies of the five-dimensional small and large Kerr-anti-de Sitter (Kerr-AdS₅) black hole with equal and unequal rotations. Our investigation also covers low and high Hawking temperatures. We then study the stability of the Kerr-AdS₅ black hole and the structure of highly damped QN modes, which would reflect the thermodynamic property of the Kerr-AdS₅ black hole. We find that the highly damped complex QN frequencies of a nearly maximally spinning Kerr-AdS₅ black hole have the periodic separation of the surface gravity at the horizon in the imaginary part while the real part converges to the superradiant frequency, which may be relevant to the pole structure of the thermal Green's function in the corresponding conformal field theory on the Kerr-AdS₅ boundary. Finally, we discuss a relation between the QN modes of the Kerr-AdS₅ black hole and the Hod's conjecture on the horizon area quantization along with the analysis of the horizon topology of the Kerr-AdS₅ black hole. We show that in general, an ultraspinning Kerr-AdS₅ black hole, whose spin parameter is infinitesimally close to the AdS curvature radius, has its noncompact horizon, and based on the Hod's conjecture, we argue that the horizon area may be continuous, that is, the unit area of the horizon vanishes in the ultraspinning regime.

DOI: [10.1103/PhysRevD.105.124044](https://doi.org/10.1103/PhysRevD.105.124044)

I. INTRODUCTION

Higher-dimensional gravity is important in the holographic principle [1–4], the braneworld scenario [5–9], and the landscape [10] of the string theory. In these contexts, black holes in higher dimensions play pivotal roles, e.g., thermality of the conformal field theory (CFT) on the anti-de Sitter (AdS) boundary [11,12], the source of dark radiation in braneworld models [13–15], and so on. Another interesting aspect of higher-dimensional black holes is that there is no corresponding theorem to a uniqueness theorem, which states that the stationary and asymptotically flat black hole is described by the Kerr solution in four-dimensional spacetime. In higher-dimensional spacetime, many black objects can exist, and their stability is an open problem. The analysis of quasinormal (QN) modes of black holes is a good probe to see its stability. The positivity of the imaginary part of complex QN frequencies leads to the exponential growth of the perturbation of black holes. The structure of QN modes is also relevant to the context of the holography as the QN

modes of black holes in AdS space are conjectured to be dual with the poles of Green's function of the CFT on the AdS boundary (see Ref. [16] for the simplest case of the duality in the BTZ black hole). The structure of QN modes of black holes could shed light on the quantum nature of black hole horizons as well. According to the Hod's conjecture [17], the real part of highly damped QN frequencies determines the unit area of a horizon. It would be an interesting question if the concept of the horizon area quantization can be extended to higher-dimensional gravity for which there are rich structures such as black holes, black rings, black strings, and so on.

In this work, we consider the QN frequencies of a scalar field in the Kerr-AdS₅ spacetime [18,19] to understand the stability, thermality, and area quantization of the black hole horizon. The scalar perturbations of the Kerr-AdS₅ black hole are governed by the Klein-Gordon equation that reduces to the Heun's differential equation by performing the coordinate transformations and the redefinition of the perturbation variables [20]. Therefore, the solution of the equation is represented by the Heun function.

The analysis of AdS₅ spacetime with a black hole and/or compactified extradimensional space has been done mainly for holographic applications [21–25]. Analytical and numerical studies of the QN modes of the Kerr-AdS₅ spacetime have been recently done in Refs. [26–30] by performing the expansion of the τ -function for the Painlevé

Published by the American Physical Society under the terms of the Creative Commons Attribution 4.0 International license. Further distribution of this work must maintain attribution to the author(s) and the published article's title, journal citation, and DOI. Funded by SCOAP³.

transcendents. In special cases, e.g., nearly equal spins, small spins, near extremal, or small mass regimes, the expansion of the τ -function converges fast and makes the computation of QN frequencies tractable. On the other hand, in our computation, we use the solution of the Teukolsky equations represented by the Heun functions, which makes the computation of the QN modes substantially fast, and allows us to investigate broader parameter regions of the Kerr-AdS₅ spacetime. Our investigation covers not only small black holes that in general lead to instability but also large black holes that are stable against linear perturbations. Also, our computation can be applied to search for not only the fundamental QN mode but also other overtones, including highly damped modes. Our computation with those advantages allows us to make a “global map” of the locations of QN modes of Kerr-AdS₅

spacetime, which would be useful to understand the stability of the background spacetime and even the Kerr-AdS/CFT correspondence [31].

In the next section, we provide a review of the scalar perturbation of the Kerr-AdS₅ black hole. In Sec. III, we study the QN modes of the Kerr-AdS₅ black hole with equal spins in the small and large mass regimes. In Sec. IV, we investigate the QN modes for the unequal spins in the small and large mass regimes. In Sec. V, we discuss some implications to the area quantization of the Kerr-AdS₅ black hole by applying the Hod’s conjecture to our results. Also, we analyze the topology of the horizon of the Kerr-AdS₅ black hole in the ultraspinning limit for which its spin parameter is infinitesimally close to the AdS curvature radius ℓ . Finally, we summarize our results and conclusions in Sec. VI.

II. FORMALISM

The Kerr-AdS₅ spacetime has the following metric

$$\begin{aligned}
 ds^2 = & -\frac{\Delta_r}{\rho^2} \left(dt - \frac{a_1 \sin^2 \theta}{1 - a_1^2} d\phi - \frac{a_2 \cos^2 \theta}{1 - a_2^2} d\psi \right)^2 + \frac{\Delta_\theta \sin^2 \theta}{\rho^2} \left(a_1 dt - \frac{r^2 + a_1^2}{1 - a_1^2} d\phi \right)^2 \\
 & + \frac{1 + r^2}{r^2 \rho^2} \left(a_1 a_2 dt - \frac{a_2 (r^2 + a_1^2) \sin^2 \theta}{1 - a_1^2} d\phi - \frac{a_1 (r^2 + a_2^2) \cos^2 \theta}{1 - a_2^2} d\psi \right)^2 \\
 & + \frac{\Delta_\theta \cos^2 \theta}{\rho^2} \left(a_2 dt - \frac{r^2 + a_2^2}{1 - a_2^2} d\psi \right)^2 + \frac{\rho^2}{\Delta_r} dr^2 + \frac{\rho^2}{\Delta_\theta} d\theta^2,
 \end{aligned} \tag{1}$$

where M is the mass parameter, the AdS curvature radius is set to $\ell = 1$, a_1 and a_2 are the spin parameters for the two rotations of the Kerr-AdS₅ black hole, and

$$\Delta_r \equiv \frac{1}{r^2} (r^2 + a_1^2)(r^2 + a_2^2)(1 + r^2) - 2M, \tag{2}$$

$$\Delta_\theta \equiv 1 - a_1^2 \cos^2 \theta - a_2^2 \sin^2 \theta, \tag{3}$$

$$\rho^2 \equiv r^2 + a_1^2 \cos^2 \theta + a_2^2 \sin^2 \theta. \tag{4}$$

Based on the thermodynamic description of the Kerr-AdS₅ spacetime, the Arnowitt-Deser-Misner (ADM) mass and angular momentum are given by [32–34]

$$\mathcal{M} \equiv \frac{\pi M (2\Xi_1 + 2\Xi_2 - \Xi_1 \Xi_2)}{4\Xi_1^2 \Xi_2^2}, \quad \mathcal{J}_\phi \equiv \frac{\pi M a_1}{2\Xi_1^2 \Xi_2}, \quad \mathcal{J}_\psi \equiv \frac{\pi M a_2}{2\Xi_1 \Xi_2^2}, \tag{5}$$

where $\Xi_i \equiv 1 - a_i^2$ ($i = 1, 2$). The spin parameters are restricted to $a_i \leq 1$, for which all the physical quantities in (5) are well-defined. We here compute the QN modes of the Kerr-AdS₅ black hole and investigate the instability of a scalar field $\Phi(t, r, \theta, \phi, \psi)$ with mass μ . Let us start with the Klein-Gordon equation

$$[\square - \mu^2]\Phi = 0, \tag{6}$$

and decomposing Ψ as $\Psi = e^{-i\omega t + im_1 \phi + im_2 \psi} \Theta(\theta) \Pi(r)$, one has the radial and angular equations:

$$\frac{1}{r} \frac{d}{dr} \left(r \Delta_r \frac{d\Pi(r)}{dr} \right) - \left[\lambda + \mu^2 r^2 + \frac{1}{r^2} (a_1 a_2 \omega - a_2 (1 - a_1^2) m_1 - a_1 (1 - a_2^2) m_2)^2 \right] \Pi(r) + \frac{(r^2 + a_1^2)^2 (r^2 + a_2^2)^2}{r^4 \Delta_r} \left(\omega - \frac{m_1 a_1 (1 - a_1^2)}{r^2 + a_1^2} - \frac{m_2 a_2 (1 - a_2^2)}{r^2 + a_2^2} \right)^2 \Pi(r) = 0, \quad (7)$$

$$\frac{1}{\sin \theta \cos \theta} \frac{d}{d\theta} \left(\sin \theta \cos \theta \Delta_\theta \frac{d\Theta(\theta)}{d\theta} \right) - \left[-\lambda + \omega^2 + \frac{(1 - a_1^2) m_1^2}{\sin^2 \theta} + \frac{(1 - a_2^2) m_2^2}{\cos^2 \theta} - \frac{(1 - a_1^2)(1 - a_2^2)}{\Delta_\theta} (\omega + m_1 a_1 + m_2 a_2)^2 + \mu^2 (a_1^2 \cos^2 \theta + a_2^2 \sin^2 \theta) \right] \Theta(\theta) = 0, \quad (8)$$

where λ is the separation constant to be determined so that $\Theta(\theta)$ is regular at $\theta = 0$ and $\theta = \pi/2$ [20]. Performing the following transformations:

$$r \rightarrow z \equiv \frac{r^2 - r_-^2}{r^2 - r_0^2}, \quad (9)$$

$$\Pi(r) \rightarrow R(z) \equiv z^{\theta_-/2} (z - z_0)^{\theta_+/2} (z - 1)^{-\Delta/2} \Pi(z), \quad z_0 \equiv \frac{r_+^2 - r_-^2}{r_+^2 - r_0^2}, \quad (10)$$

$$\sin^2 \theta \rightarrow u \equiv \frac{\sin^2 \theta}{\sin^2 \theta - \chi_0}, \quad \text{with } \chi_0 \equiv \frac{1 - a_1^2}{a_2^2 - a_1^2}, \quad (11)$$

$$\Theta(\theta) \rightarrow S(u) \equiv u^{-m_1/2} (u - 1)^{-\Delta/2} (u - u_0)^{-m_2/2} \Theta(u), \quad (12)$$

with r_- and r_+ being the inner and outer horizon radii, respectively, r_0 being the imaginary root of Δ_r , $\Delta \equiv 2 + \sqrt{4 + \mu^2}$, and $u_0 \equiv (a_2^2 - a_1^2)/(a_2^2 - 1)$, the radial and angular equations reduce to the Heun's differential equations:

$$\frac{d^2 R}{dz^2} + \left[\frac{1 - \theta_-}{z} + \frac{-1 + \Delta}{z - 1} + \frac{1 - \theta_+}{z - z_0} \right] \frac{dR}{dz} + \left(\frac{\kappa_1 \kappa_2}{z(z - 1)} - \frac{K}{z(z - 1)(z - z_0)} \right) R = 0, \quad (13)$$

$$\frac{d^2 S}{du^2} + \left[\frac{1 + m_1}{u} + \frac{-1 + \Delta}{u - 1} + \frac{1 + m_2}{u - u_0} \right] \frac{dS}{du} + \left(\frac{q_1 q_2}{u(u - 1)} - \frac{Q}{u(u - 1)(u - u_0)} \right) S = 0, \quad (14)$$

where

$$\theta_i \equiv \frac{i}{2\pi} \frac{\omega - m_1 \Omega_{i,1} - m_2 \Omega_{i,2}}{T_i}, \quad (15)$$

$$T_i \equiv \frac{r_i^2 \Delta'_r(r_i)}{4\pi(r_i^2 + a_1^2)(r_i^2 + a_2^2)}, \quad \Omega_{i,1} \equiv \frac{a_1 \Xi_1}{r_i^2 + a_1^2}, \quad \Omega_{i,2} \equiv \frac{a_2 \Xi_2}{r_i^2 + a_2^2}, \quad (16)$$

$$\kappa_1 \equiv -\frac{1}{2} (\theta_- + \theta_+ - \Delta - \theta_0), \quad \kappa_2 \equiv -\frac{1}{2} (\theta_- + \theta_+ - \Delta + \theta_0), \quad (17)$$

$$q_1 \equiv \frac{1}{2} (m_1 + m_2 + \Delta - \zeta), \quad q_2 \equiv \frac{1}{2} (m_1 + m_2 + \Delta + \zeta), \quad (18)$$

$$\zeta \equiv \omega + a_1 m_1 + a_2 m_2, \quad (19)$$

$$K \equiv -\frac{1}{4} \left\{ \frac{\lambda + \mu^2 r_-^2 - \omega^2}{r_+^2 - r_0^2} + (z_0 - 1)[(\theta_+ + \theta_- - 1)^2 - \theta_0^2 - 1] + z_0 [2(\theta_+ - 1)(1 - \Delta) + (2 - \Delta)^2 - 2] \right\}, \quad (20)$$

$$Q \equiv -\frac{1}{4} \left\{ \frac{\omega^2 + a_1^2 \mu^2 - \lambda}{a_2^2 - 1} + u_0 [(m_2 + \Delta - 1)^2 - m_2^2 - 1] + (u_0 - 1) [(m_1 + m_2 + 1)^2 - \zeta^2 - 1] \right\}. \quad (21)$$

The general solution of the Heun's differential equation, (13), is

$$\begin{aligned} R &= c_0 R_{\text{in}}(\omega, z) + d_0 R_{\text{out}}(\omega, z) \\ &\equiv c_0 H\ell \left(\frac{z_0}{z_0 - 1}, \frac{-K}{z_0 - 1}; \kappa_1, \kappa_2, 1 - \theta_+, \Delta - 1; \frac{z_0 - z}{z_0 - 1} \right) \\ &\quad + d_0 \left(\frac{z_0 - z}{z_0 - 1} \right)^{\theta_+} H\ell \left(\frac{z_0}{z_0 - 1}, \frac{\theta_+ [z_0(\Delta - \theta_-) - 1 + \theta_-]}{z_0 - 1} - \frac{K}{z_0 - 1}; \kappa_1 + \theta_+, \kappa_2 + \theta_+, 1 + \theta_+, \Delta - 1; \frac{z_0 - z}{z_0 - 1} \right), \end{aligned} \quad (22)$$

for $z \sim z_0$ ($r \sim r_+$), and

$$\begin{aligned} R &= c_1 R_{\text{AdS}}(\omega, z) + d_1 R_{\text{Div}}(\omega, z) \\ &\equiv c_1 H\ell(1 - z_0, \kappa_1 \kappa_2 - \tilde{K}; \kappa_1, \kappa_2, \Delta - 1, 1 - \theta_-; 1 - z) \\ &\quad + d_1 (1 - z)^{2 - \Delta} H\ell(1 - z_0, [(1 - z_0)(1 - \theta_-) + 1 - \theta_+](2 - \Delta) + \kappa_1 \kappa_2 - \tilde{K}; \\ &\quad \kappa_1 + 2 - \Delta, \kappa_2 + 2 - \Delta, 3 - \Delta, 1 - \theta_-; 1 - z), \end{aligned} \quad (23)$$

for $z \sim 1$ ($r \sim \infty$). Here c_i and d_i ($i = 0, 1$) are arbitrary constants and we define $\tilde{K} \equiv K + \kappa_1 \kappa_2 z_0$. For the angular equation (14), its general solution is

$$\begin{aligned} S &= \tilde{c}_0 H\ell(u_0, \tilde{Q}; q_1, q_2, 1 + m_1, \Delta - 1; u) + \tilde{d}_0 z^{m_1} H\ell(u_0, \tilde{Q} - m_1 [u_0(\Delta - 1) + m_2 + 1]; \\ &\quad q_1 - m_1, q_2 - m_1, 1 - m_1, \Delta - 1; u) \end{aligned} \quad (24)$$

around $u \sim 0$ ($\theta \sim 0$), and

$$\begin{aligned} S &= \tilde{c}_1 H\ell \left(\frac{u_0}{u_0 - 1}, \frac{-Q}{u_0 - 1}; q_1, q_2, 1 + m_2, \Delta - 1; \frac{u_0 - u}{u_0 - 1} \right) \\ &\quad + \tilde{d}_1 \left(\frac{u_0 - u}{u_0 - 1} \right)^{-m_2} H\ell \left(\frac{u_0}{u_0 - 1}, \frac{-Q - m_2 [u_0(\Delta + m_1) - (1 + m_1)]}{u_0 - 1}; \right. \\ &\quad \left. q_1 - m_2, q_2 - m_2, 1 - m_2, \Delta - 1; \frac{u_0 - u}{u_0 - 1} \right) \end{aligned} \quad (25)$$

around $u \sim u_0$ ($\theta \sim \pi/2$), where \tilde{c}_i and \tilde{d}_i ($i = 0, 1$) are arbitrary constants and $\tilde{Q} \equiv Q + q_1 q_2 u_0$. To ensure the ingoing and Dirichlet boundary conditions at $r = r_+$ and $r = \infty$, respectively, one has to impose the following boundary condition for $\Pi(z)$

$$\Pi(z) \sim \begin{cases} (z - z_0)^{-\theta_+/2} & \text{for } z \rightarrow z_0 (r \rightarrow r_+), \\ (z - 1)^{\Delta/2} & \text{for } z \rightarrow 1 (r \rightarrow \infty), \end{cases} \quad (26)$$

and for $\Theta(u)$, the regular condition at $u = 0$ ($\theta = 0$) and $u = u_0$ ($\theta = \pi/2$) is

$$\Theta(u) \sim \begin{cases} u^{|m_1|/2} & \text{for } u \rightarrow 0, \\ (u - u_0)^{|m_2|/2} & \text{for } u \rightarrow u_0. \end{cases} \quad (27)$$

To satisfy the boundary condition (26), $R(z)$ should take the following form at the boundaries

$$R \sim R_{\text{in}}(\omega, z) \quad \text{for } z \sim z_0, \quad (28)$$

$$R \sim R_{\text{AdS}}(\omega, z) \quad \text{for } z \sim 1. \quad (29)$$

For $u \sim 0$, on the other hand, $S(u)$ takes the following form

$$S = S_0 \equiv \begin{cases} H\ell(u_0, \tilde{Q}; q_1, q_2, 1 + m_1, \Delta - 1; u) & \text{for } m_1 \geq 0, \\ z^{-m_1} H\ell(u_0, -m_1[u_0(\Delta - 1) + 1 + m_2] + \tilde{Q}; q_1 - m_1, q_2 - m_1, 1 - m_1, \Delta - 1; u) & \text{for } m_1 \leq 0, \end{cases} \quad (30)$$

and for $u \sim u_0$, $S(u)$ is

$$S = S_{u_0} \equiv \begin{cases} H\ell\left(\frac{u_0}{u_0-1}, \frac{q_1 q_2 u_0 - \tilde{Q}}{u_0-1}; q_1, q_2, 1 + m_2, \Delta - 1; \frac{u_0-u}{u_0-1}\right) & \text{for } m_2 \geq 0 \\ \left(\frac{u_0-u}{u_0-1}\right)^{-m_2} H\ell\left(\frac{u_0}{u_0-1}, \frac{-m_2[u_0(m_1+\Delta)-1-m_1] + q_1 q_2 u_0 - \tilde{Q}}{u_0-1}; q_1 - m_2, q_2 - m_2, 1 - m_2, \Delta - 1; \frac{u_0-u}{u_0-1}\right) & \text{for } m_2 \leq 0. \end{cases} \quad (31)$$

In the following sections, we use the *Wolfram Mathematica* to search for the eigenvalues $\lambda_{lm_1 m_2 n}$ and QN frequencies $\omega_{lm_1 m_2 n}$ for which the boundary conditions (28)–(31) are satisfied. Note that a function $\text{HeunG}[\bar{a}, \bar{q}, \bar{\alpha}, \bar{\beta}, \bar{\gamma}, \bar{\delta}, x]$ in *Mathematica* is not defined for a nonpositive integer of $\bar{\gamma}$ as the power expansion of the Heun function is singular in such a case. Therefore, R_{Div} in (23) cannot be defined in *Mathematica* when $\Delta = n_*$ with $n_* \in \{4, 5, 6, \dots\}$. Nevertheless, this does not affect our numerical computation to find QN frequencies because our computation searches for the zeros of the Wronskian of R_{in} and R_{AdS} , both of which are well defined even for $\Delta = n_*$. More details of our computation including its accuracy are discussed in Appendix.

III. STABILITY ANALYSIS FOR EQUAL SPINS ($a_1 = a_2$)

In this section, we numerically investigate the QN frequencies for a Kerr-AdS₅ black hole with $a_1 = a_2 \equiv a$. For equal spins, the angular equation reduces to the hypergeometric differential equation, and one can obtain the analytic expression of the eigenvalue λ [20]

$$\lambda = (1 - a^2)[l(l+2) - 2\omega a(m_1 + m_2) - a^2(m_1 + m_2)^2] + a^2\omega^2 + a^2\Delta(\Delta - 4), \quad (32)$$

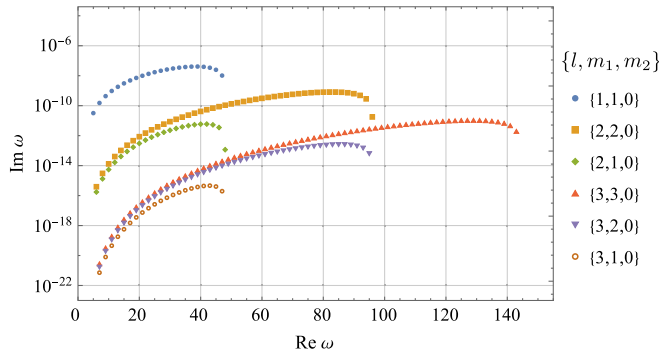


FIG. 1. Each point represents a QN frequency, $\omega_{lm_1 m_2 n}$, and unstable overtones, labeled by n , are plotted for each harmonic mode (l, m_1, m_2) . We set $a_1 = a_2 = 4 \times 10^{-4}$, $\mathcal{M} = 10^{-5}$ and $\mu = 10^{-2}$.

where $l = 0, 1, 2, \dots$ is the angular mode. We can obtain QN frequencies by solving the radial equation (13) with $\lambda = \lambda(\omega)$ given in (32) and by searching for $\omega = \omega_{lm_1 m_2 n}$ at which the obtained solution satisfies the boundary condition (26).

A. Small black holes $\mathcal{M} \ll 1$

For small black holes, QN frequencies are localized near the real axis of the complex frequency plane, $|\text{Re}(\omega_{lm_1 m_2 n})| \gg |\text{Im}(\omega_{lm_1 m_2 n})|$, due to trapped modes in the AdS boundary. Also, the superradiant instability is caused by the resonance between the ergoregion and AdS boundary. The stability of the black hole can be read from the sign of the imaginary part of QN frequencies, and $\text{Im}(\omega_{lm_1 m_2 n}) > 0$ means that the background spacetime is unstable against linear perturbations. For small Kerr-AdS₅ black holes, the unstable QN modes satisfy the following condition

$$\text{Re}(\omega_{lm_1 m_2 n}) < m_1 \Omega_{+,1} + m_2 \Omega_{+,2} \equiv \Omega. \quad (33)$$

Here it is natural to ask which overtone leads to the most significant instability when multiple overtones satisfy the above condition. To see this, we first investigate QN modes for $l = 1, 2, 3$ in Fig. 1, and it is found that $l = 1$ mode leads to the most significant instability. We then study the spin-dependence of QN modes with $(l, m_1, m_2) = (1, 1, 0)$, and the result is shown in Fig. 2. It is shown that rapid rotations destabilize the Kerr-AdS₅ black holes, and the peak of $\text{Im}(\omega_{lm_1 m_2 n})$ is slightly below the superradiant frequency of Ω . We also confirm that our result shown in Fig. 2 is consistent with the condition of the superradiant instability (33) as $\text{Re}(\omega_{lm_1 m_2 n}) < 136.422$ and $\text{Re}(\omega_{lm_1 m_2 n}) < 11.795$ for $a = 10^{-3}$ and $a = 10^{-4}$, respectively.¹ In the following, we will omit the subscript $+$ from $\Omega_{+,i}$. Besides the QN modes localized near the real axis of ω , highly

¹Note that fixing the spin and mass parameters, a_i and M , is equivalent to fixing the ADM mass and angular momenta shown in (5). Also, the angular momenta, $J_\phi(M, a_i)$ and $J_\psi(M, a_i)$, are monotonically increasing functions with respect to a_i when $a_i \leq 1$.

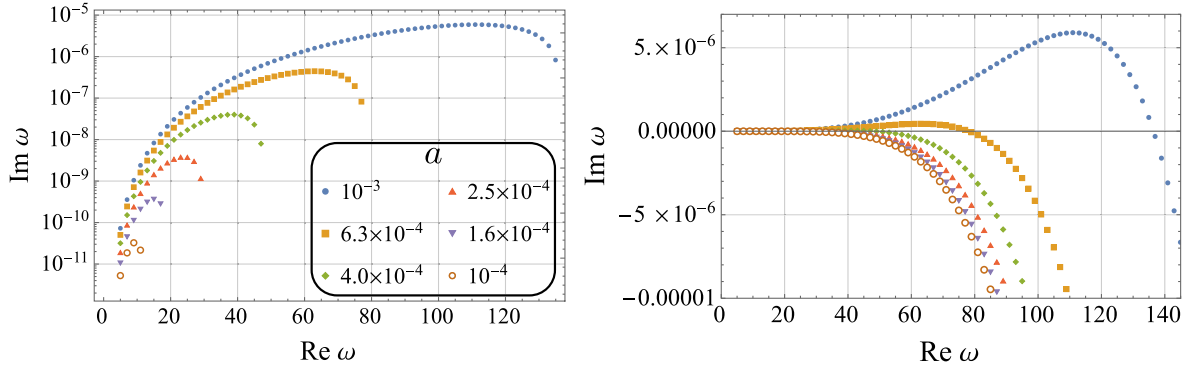


FIG. 2. Plot of QN frequencies for various spin parameters. In the left and right panels, the imaginary part is shown in log and linear scale, respectively. Each marker indicates the complex value of each QN frequency. We set $\mathcal{M} = 10^{-5}$ and $\mu = 10^{-2}$, and the spin parameters are in the range of $10^{-4} \leq a (= a_1 = a_2) \leq 10^{-3}$. The angular modes are fixed as $(l, m_1, m_2) = (1, 1, 0)$ that is equivalent to $(1, 0, 1)$.

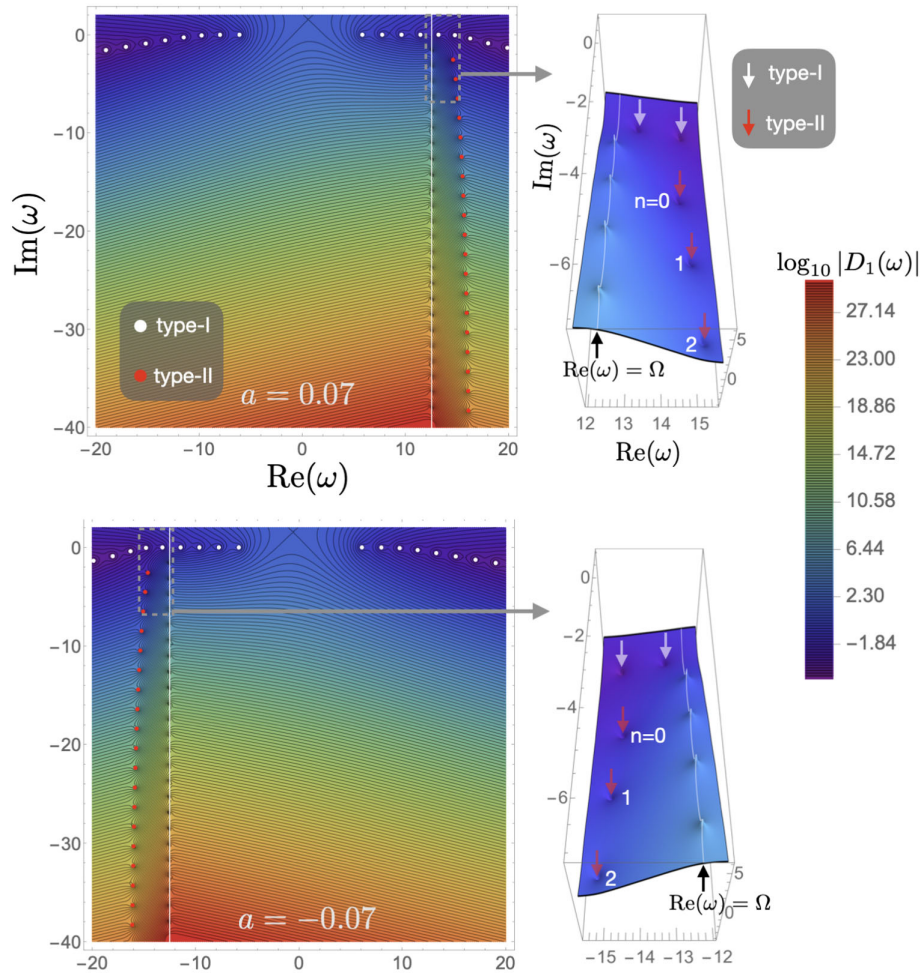


FIG. 3. Plots of the coefficient $|D_1(\omega)|$ defined in (34). The parameters are set to $a = \pm 0.07$, $M = 0.01$, and $(l, m_1, m_2) = (2, 1, 1)$. The type-II modes are numbered by non-negative integers, n , in ascending order of the damping rates.

damped QN modes are localized near the line of $\text{Re}(\omega) = \Omega$ in the complex frequency plane, as is shown in Fig. 3. The coefficient $D_1(\omega)$, defined as

$$R_{\text{BH}}(\omega, z) = C_1(\omega)R_{\text{AdS}}(\omega, z) + D_1(\omega)R_{\text{Div}}(\omega, z), \quad (34)$$

is plotted in Fig. 3, and it vanishes at $\omega = \omega_{lm_1m_2n}$. Hereinafter, we call QN modes localized near the real axis of ω and those localized near the superradiant frequency *type I* and *type II*, respectively. The type-I modes are caused by the resonance between the AdS barrier and the angular momentum barrier. On the other hand, type-II modes may be relevant to the thermality of the Kerr-AdS₅ black hole as their separation in frequency space is nearly equal to the surface gravity of Kerr-AdS₅ black hole $2\pi T_{\text{H}}$, and the real part of the type-II modes can be interpreted as the chemical potential. Figure 4 shows the trajectories of the type-I and type-II modes with respect to the change of the Hawking temperature. One can see that the lower the Hawking temperature of the Kerr-AdS₅ black hole is, the stronger the localization of type-II modes at the superradiant frequency is (see Fig. 5). Also, the separation of the imaginary part of QN frequencies, defined as $\Delta\text{Im}(\omega_{lm_1m_2n}) \equiv \text{Im}(\omega_{lm_1m_2n} - \omega_{lm_1m_2(n+1)})$, approaches $2\pi T_{\text{H}}$ in the zero-temperature limit. It looks like

the behaviors of highly damped QN modes are insensitive to μ at least for $0.01 \leq \mu \leq 10$.

In the next subsection, we will see the massive case, $\mathcal{M} \gtrsim 1$, for which the lowest Hawking temperature is nonzero and finite due to the upper bound on the two spins ($a_i \leq 1$ with $i = 1, 2$). We will show the structure of the type-II modes in the complex frequency plane for the lowest Hawking temperature.

B. Large black holes $\mathcal{M} \gtrsim 1$

Massive Kerr-AdS₅ black holes ($\mathcal{M} \gtrsim 1$) are stable against linear perturbations, which is equivalent to $\text{Im}(\omega_{lm_1m_2n}) < 0$ for all modes, since the cavity between the angular momentum barrier of the black hole and the AdS boundary to cause the resonant instability does not exist for massive black holes. The trajectories of QN modes for $M = 5$ is shown in Fig. 6. Note that type-I modes (dashed lines) correspond to the QN modes that localize near the real axis of ω in the small mass regime (cf. Sec. III A). In that case, the type-I modes are caused by the resonance in the AdS boundary, and thus, the type-I modes periodically appear near the real axis of ω , which is similar to the normal modes of a vibrating string. In the massive case, on the other hand, type-I modes are highly suppressed especially for $a \rightarrow 1$, while type-II modes

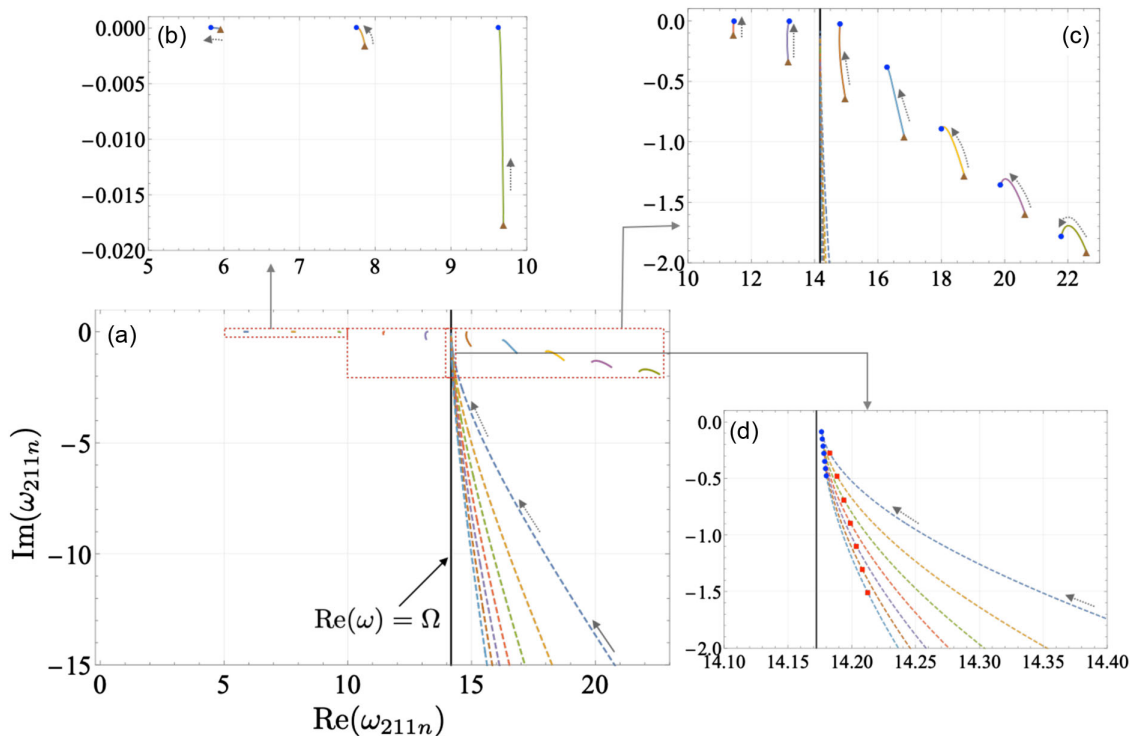


FIG. 4. Trajectories of QN frequencies for $M = 0.01$, $(l, m_1, m_2) = (2, 1, 1)$, and $\mu = 0.01$. The solid and dashed lines indicate the type-I and type-II QN modes, respectively. The spin parameter a runs from $a = 10^{-4}$ (brown triangles) to $a \simeq 0.999996a_{\text{max}}$ (blue dots) in (b) and (c). The spin parameter runs up to $a = 0.99999a_{\text{max}}$ (blue dots) in (d). The maximum spin parameter is $a_{\text{max}} = 0.070536282\dots$ and the red squares in (d) indicate the QN frequencies at $a = 0.07$. The arrows indicate the direction in which the spin parameter, a , increases.

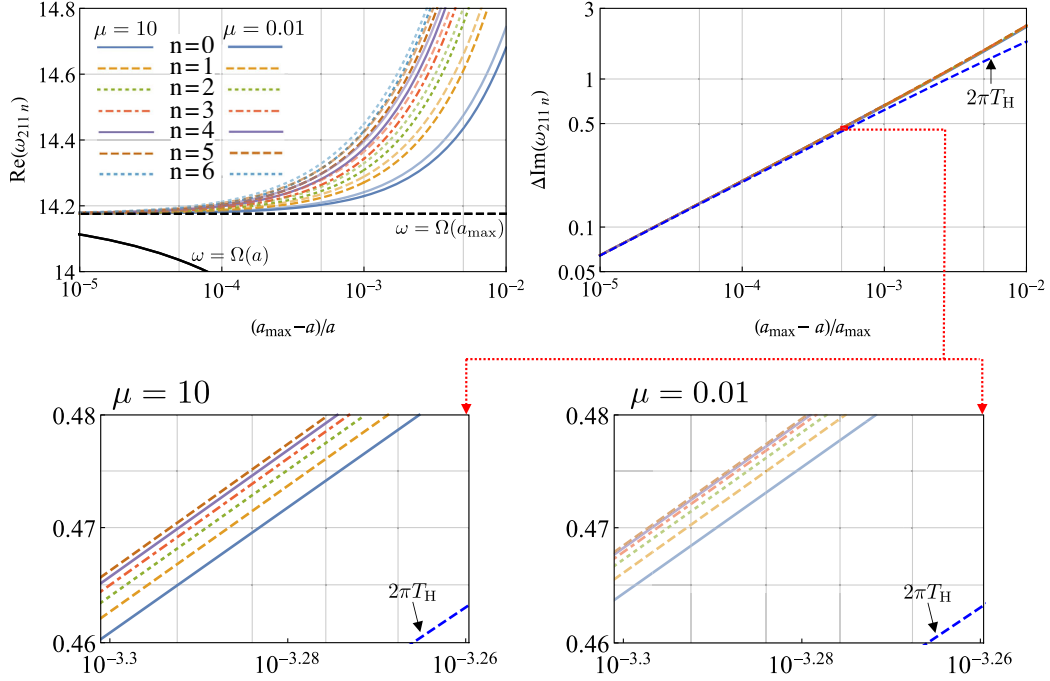


FIG. 5. The real part and the separation in the imaginary part of QN frequencies are shown with respect to $(a_{\max} - a)/a_{\max}$ in the upper left and upper right panels, respectively. We change the opacity of each line to distinguish the case of $\mu = 0.01$ (transparent lines) and $\mu = 10$ (opaque lines). The other parameters are set to $M = 0.01$ and $(l, m_1, m_2) = (2, 1, 1)$. In the left panel, the black solid line indicates the superradiant frequency, Ω , that depends on a , and the black dashed line shows the value of Ω at the extremal case ($a = a_{\max}$). The blue dashed line in the right panel is $2\pi T_H(a)$. As a reference, the region of $10^{-3.3} \leq (a_{\max} - a)/a_{\max} \leq 10^{-3.26}$ is zoomed in and displayed in the lower panels.

localize at $\text{Re}(\omega) = \Omega$ (see Fig. 6). Note that in the limit of $a \rightarrow 1$, the superradiant frequency also vanishes $\Omega \propto (1 - a^2) \rightarrow 0$. We also find that the type-II modes appear from the region of $\text{Re}(\omega) > \Omega$ for $a > 0$ and they do from the region of $\text{Re}(\omega) < \Omega$ for the counterrotations ($a < 0$), as is shown in Fig. 7, where the absolute value of $|D_1(\omega)|$ is shown in the log-scale.

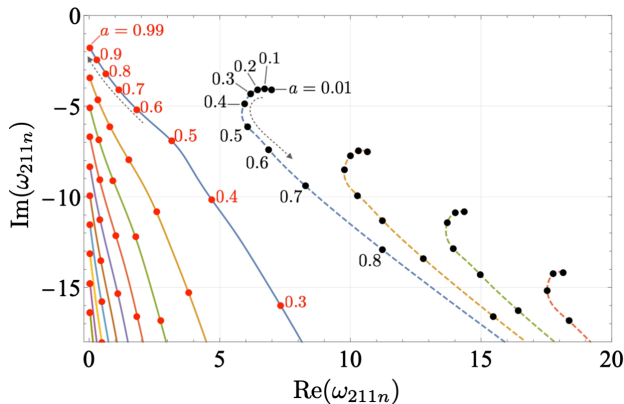


FIG. 6. Trajectories of QN frequencies for $M = 5$ and $(l, m_1, m_2) = (2, 1, 1)$. The spin parameter a runs from $a = 0.01$ to $a = 0.99$. The dashed and solid lines indicate the type-I and type-II QN modes, respectively. The arrows indicate the direction in which the spin parameter, a , increases.

We confirm that the separation $\Delta \text{Im}(\omega_{lm_1 m_2 n})$ approaches $2\pi T_H$ for $a \rightarrow 1$ as is shown in Fig. 8. It looks like the separation converges to $2\pi T_H$ for highly damped modes (higher overtone number n) though it is dispersive, and its convergence is weaker when the mass of the scalar field, μ , is massive. This implies that the convergence of $\Delta \text{Im}(\omega_{lm_1 m_2 n})$ to $2\pi T_H$ for $n \gg 1$ is delayed or that the thermality of the Kerr-AdS₅ black hole would be disturbed by the mass of surrounding fields. Figure 9 shows that nevertheless the real part of type-II modes strongly converges to the superradiant frequency Ω in the ultra-spinning limit for both small and large μ . As a final remark of this section, we have numerically computed the type-II QN frequencies up to finite overtone numbers. There is still a possibility that even high-temperature Kerr-AdS₅ black holes have the thermal structure of their QN modes at $n \rightarrow \infty$, i.e., the real part and the separation of the imaginary part of the type-II modes match Ω and $2\pi T_H$, respectively, in the highly damped limit.

IV. STABILITY ANALYSIS FOR UNEQUAL SPINS ($a_1 > a_2$)

In this section, we numerically investigate the configuration of QN modes in the complex frequency plane for Kerr-AdS₅ black holes with unequal-spin parameters $a_1 > a_2$. In this case, the symmetry of spacetime reduces

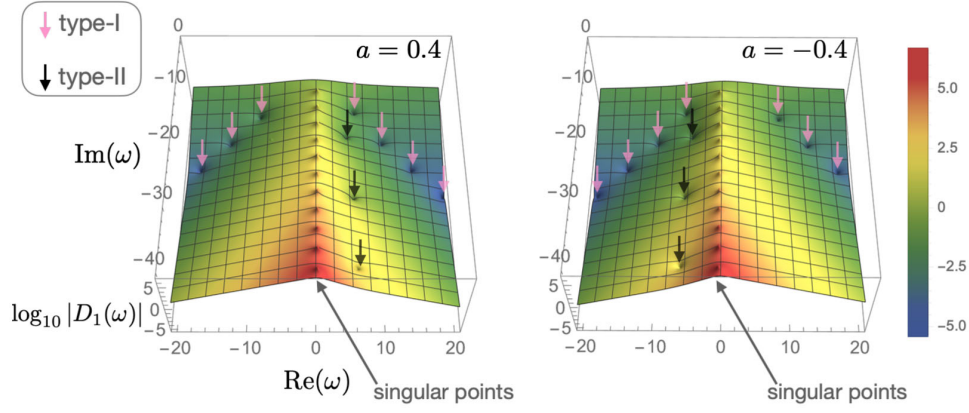


FIG. 7. 3D plots of the coefficient $|D_1(\omega)|$ in the complex frequency plane. The zeros of D_1 correspond to the complex QN frequencies, $\omega = \omega_{lm_1 m_2 n}$, and the pink and black arrows indicate the type-I and type-II modes, respectively. Here we set $(l, m_1, m_2) = (2, 1, 1)$, $M = 5$, and $\mu = 0.01$. The spins are set to $a = 0.4$ (left) and $a = -0.4$ (right).

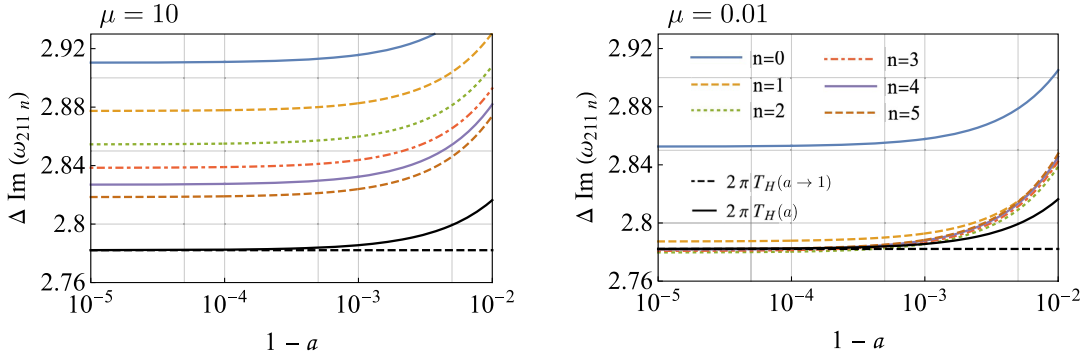


FIG. 8. Plots of $\Delta \text{Im}(\omega_{211n})$ for $\mu = 10$ (left) and $\mu = 0.01$ (right). The black line indicates $2\pi T_H(a)$, and black dashed line indicates $2\pi T_H(a \rightarrow 1)$. The other parameters are set to $M = 10$ and $(l, m_1, m_2) = (2, 1, 1)$.

to $U(1) \times U(1)$ while it is enhanced to $U(2)$ for $a_1 = a_2$. We investigate how the reduction of the symmetry affects the superradiant instability in Sec. IV A and study the structure of highly damped QN modes for unequal spins in Sec. IV B.

A. Small black holes $\mathcal{M} \ll 1$

To see which harmonic mode is the most significant to destabilize the system, we numerically compute the QN frequencies for various values of the spin ratio, a_2/a_1 . We then numerically confirm that the most dominant instability is caused by the mode of $(l, m_1, m_2) = (1, 1, 0)$ for $a_1 > a_2$ as is shown in Fig. 10. Therefore, we consider the instability of $(1, 1, 0)$ only and investigate how the reduction of the symmetry of spacetime affects the instability.² We compute the QN frequencies by fixing the ADM mass, the mass of the scalar field, and the superradiant frequency in Fig. 11. As a result, we find that the instability is more

²The opposite hierarchy between a_1 and a_2 ($a_2/a_1 > 1$) results in the suppression of the instability of $(1, 1, 0)$, and then the instability caused by $(1, 0, 1)$ mode becomes dominant.

significant when the spin ratio a_2/a_1 is smaller. Our result implies that the symmetry reduction of the Kerr-AdS₅ black hole leads to the enhancement of the superradiant instability when \mathcal{M} , μ , and Ω_1 are fixed.

We found that the structure of type-II modes exhibits the thermodynamic nature of the Kerr-AdS₅ black hole in the low-temperature or ultraspinning limits with $a_1 = a_2$ (see Sec. III A and III B). We here investigate if the thermal interpretation of the type-II modes holds even for unequal spins ($a_1 \neq a_2$). The left panel in Fig. 12 shows that the real part of type-II modes approaches the superradiant frequency for lower T_H , which is similar to the case of small Kerr-AdS₅ black holes with equal spins (see Fig. 5). From the right panel in Fig. 12, one can also see that $\Delta \text{Im}(\omega_{211n})$ matches $2\pi T_H$ in the low-temperature limit. From those results, we confirm that the thermodynamic nature of the Kerr-AdS₅ black hole we observed for the equal spin case still holds even for unequal spins.

B. Large black holes $\mathcal{M} \gtrsim 1$

We here investigate the type-II QN frequencies of a large black hole $\mathcal{M} \gtrsim 1$ with unequal spins. The Kerr-AdS₅

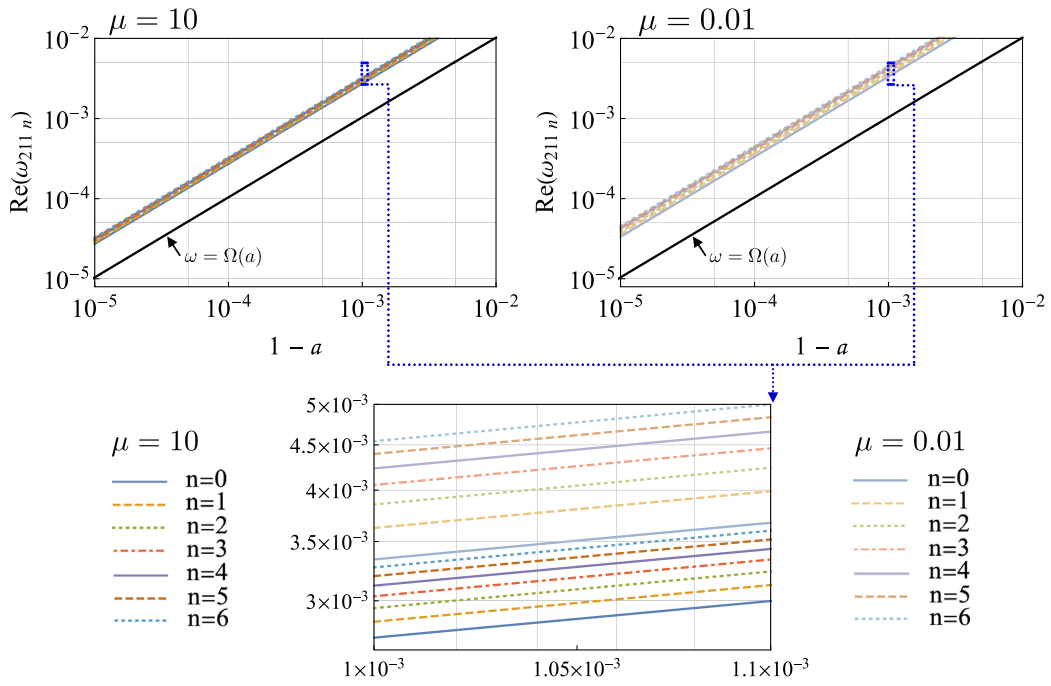


FIG. 9. Plots of $\text{Re}(\omega_{211n})$ for $\mu = 10$ (upper left) and $\mu = 0.01$ (upper right). The other parameters are set to $M = 10$ and $(l, m_1, m_2) = (2, 1, 1)$. We change the opacity of each line to distinguish the case of $\mu = 0.01$ (transparent lines) and $\mu = 10$ (opaque lines). The region of $1.0 \times 10^{-3} \leq 1-a \leq 1.1 \times 10^{-3}$ is zoomed in and displayed in the lower panel for comparison.

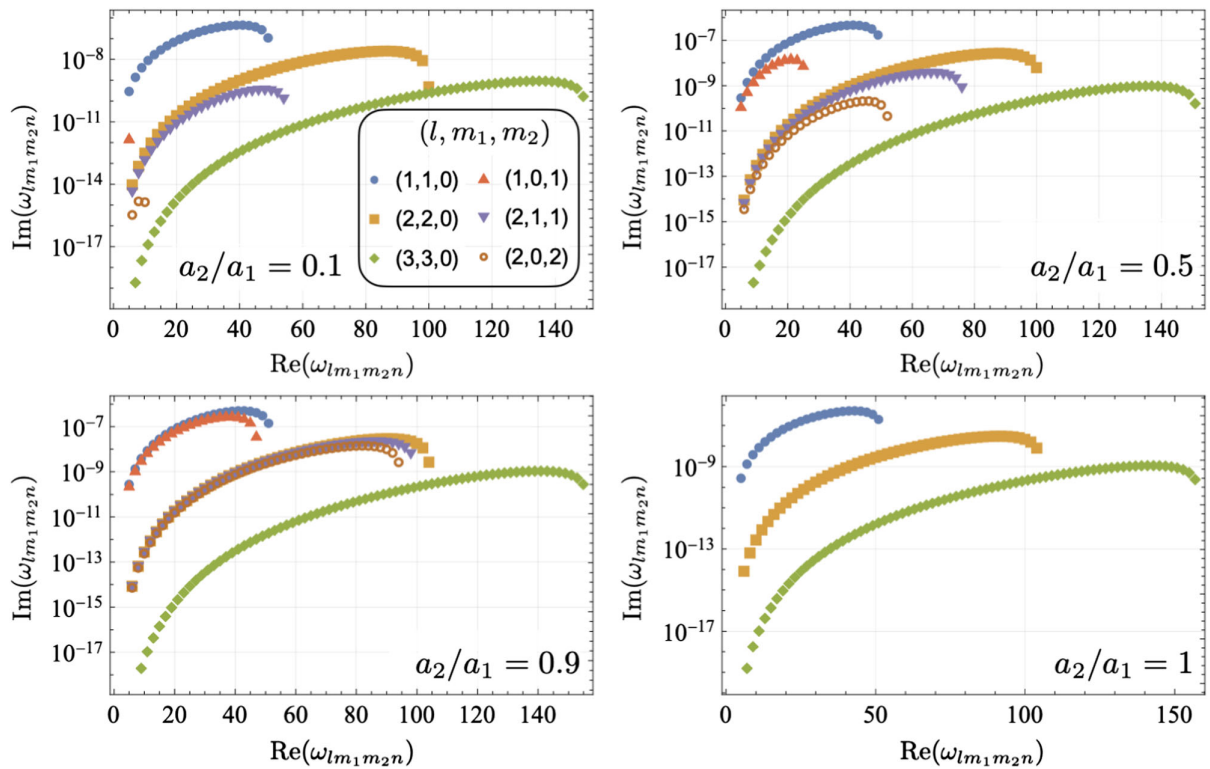


FIG. 10. QN frequencies of $l = 1, 2, 3$ modes for various ratio of spin parameters ($a_2/a_1 = 0.1, 0.5, 0.9$, and 1). We set the background metric as $M = 10^{-5}$, $\mu = 10^{-2}$, and $a_1 = 10^{-3}$.

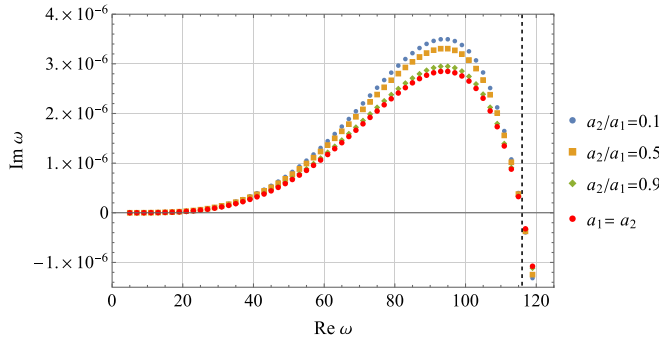


FIG. 11. Plot of QN frequencies for various values of the spin ratio. Each marker indicates the complex value of each QN frequency. We set $\mathcal{M} = 10^{-5}$, $\mu = 10^{-2}$, and superradiant frequency $\Omega = 116$, and the spin ratio is set to $a_2/a_1 = 1, 0.9, 0.5$, and 0.1 . The angular modes are fixed as $(l, m_1, m_2) = (1, 1, 0)$. The black dashed line indicates the superradiant frequency.

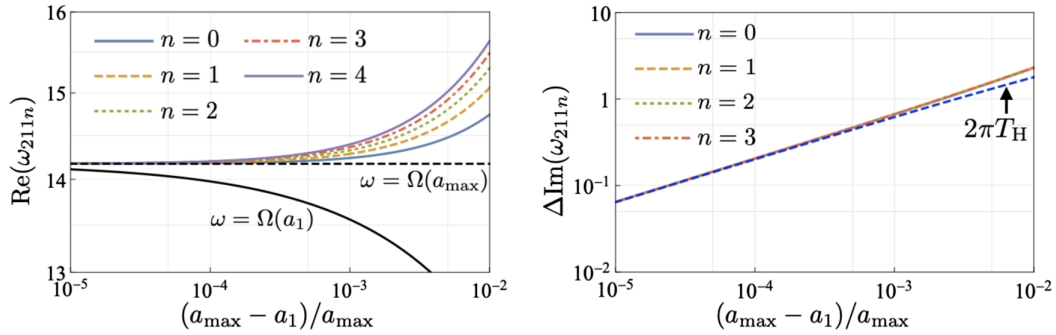


FIG. 12. The real part and the separation of the imaginary part of QN frequencies are shown with respect to $(a_{\max} - a_1)/a_{\max}$ in the left and right panels, respectively. We set $a_2/a_1 = 0.9$, $M = 0.01$, and $\mu = 0.01$. In the left panel, the black solid line indicates the superradiant frequency, Ω , that depends on a_1 , and the black dashed line shows the value of Ω at the extremal case ($a_1 = a_{\max}$). The blue dashed line in the right panel shows $2\pi T_H(a_1)$.

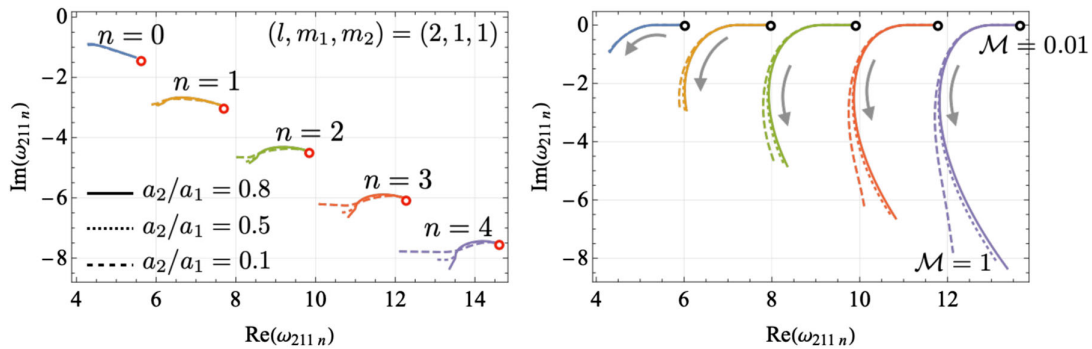


FIG. 13. Trajectories of QN frequencies in the complex frequency plane. In the left panel, we set $\mathcal{M} = 1$ and the Hawking temperature changes from the lower value of $T_H = 0.01$ to the maximum temperature while fixing the spin ratio a_2/a_1 . The red open circles indicate the QN frequencies for which T_H takes the maximum value. In the right panel, the Hawking temperature is fixed at $T_H = 0.01$ and the ADM mass changes from $\mathcal{M} = 0.01$ (black open circles) to $\mathcal{M} = 1$. The arrows indicate the direction in which the ADM mass increases. The harmonic mode is set to $(l, m_1, m_2) = (2, 1, 1)$.

spacetime is stable for $\mathcal{M} \gtrsim 1$ in the case of unequal spins, $a_1 > a_2$, as well. In Fig. 13, the QN frequencies are shown up to the 4th overtone. We can see that each QN frequency has a bent path when the Hawking temperature changes while the other quantities are fixed (left panel in Fig. 13). As a Kerr-AdS₅ black hole becomes massive, the background spacetime is getting stabilized, which can be seen in the right panel of Fig. 13 and is similar to the equal spin case.

We have numerically shown that the damping rates of the type-II QN modes of a small Kerr-AdS₅ black hole with unequal spins also have the periodicity of $2\pi T_H$. We here numerically check that the intriguing thermodynamic property of highly damped modes holds even for Kerr-AdS₅ black holes with large mass and unequal spins. We show the separation $\Delta\text{Im}(\omega_{lm_1m_2n})$ as a function of $1 - a_1$ in Fig. 14. For highly damped modes, the separation

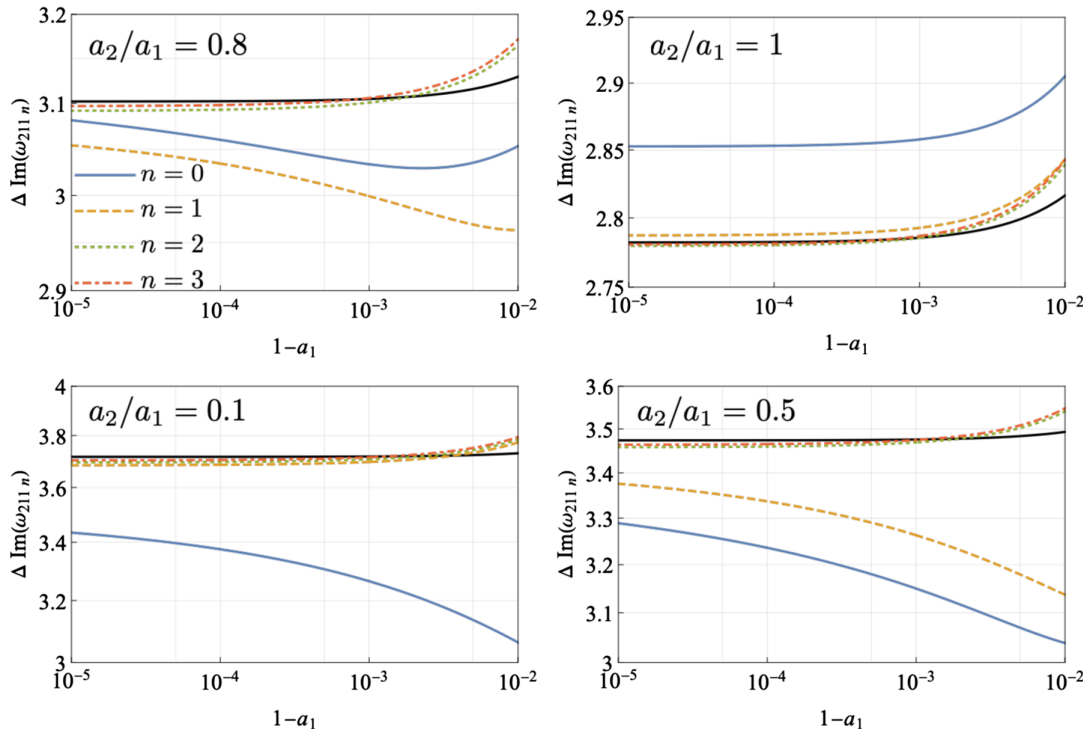


FIG. 14. The separation of the imaginary part of the type-II QN frequencies is shown as a function of $1 - a_1$ in the ultraspinning limit. The harmonic mode is set to $(l, m_1, m_2) = (2, 1, 1)$ and $M = 10$. The black solid lines show the values of $2\pi T_H(a_1)$.

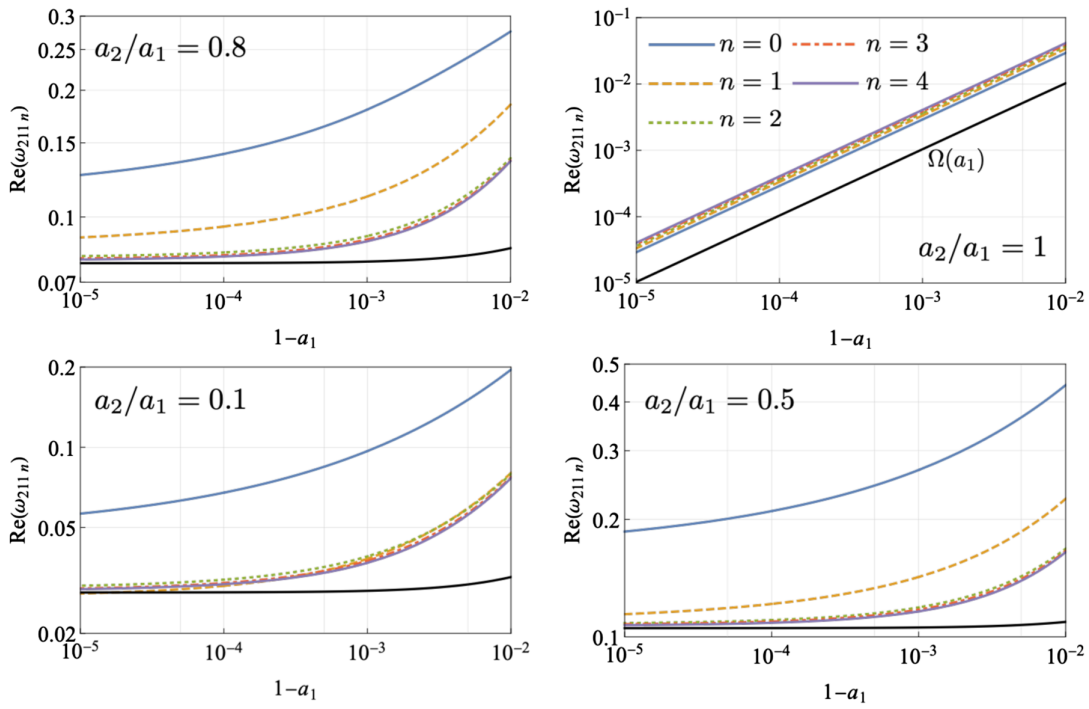


FIG. 15. Real part of the QN frequencies in the ultraspinning limit. The spin ratio is fixed as $a_2/a_1 = 0.1, 0.5, 0.8,$ and 1 , the mass parameter is $M = 10$, and the harmonic mode is $(l, m_1, m_2) = (2, 1, 1)$. The QN frequencies are shown up to the 4th overtone. For the equal spins, the real part of QN frequencies approaches zero as $\Omega \rightarrow 0$ in the ultraspinning limit. For unequal spin case, $\text{Re}(\omega_{211n})$ saturates at $\Omega > 0$. The black lines indicate the value of Ω .

approaches $2\pi T_H$ in the ultraspinning limit.³ Also, Figure 15 shows the real part of the type-II QN frequencies for up to the 4th overtone, and one can see that $\text{Re}(\omega_{lm_1m_2n})$ approaches $\text{Re}(\omega) = \Omega$ as $a_1 \rightarrow 1$. In the next section, we discuss an implication we can obtain by combining our result and the Hod's conjecture on the black hole area quantization [17].

V. AREA QUANTIZATION OF THE Kerr-AdS₅ BLACK HOLE

In the previous section, we found that the real part of the highly damped QN frequencies approaches the superradiant frequency. The strong localization at $\text{Re}(\omega) = \Omega$ can be seen in the low-temperature or ultraspinning limits. According to the Hod's conjecture [17], the asymptotic value of the real part of QN frequencies of massless fields determines the smallest size of a quantized horizon area, ΔA , and the horizon area is given by $A = N_{\text{max}} \Delta A$. The integer N_{max} is the total number of the unit area on the horizon. Although our computation has been performed mainly for⁴ $\mu = 0.01$, we confirm that the values of QN frequencies are well converged to the values for $\mu = 0$, at least in the range of $\mu \leq 0.01$ (see Fig. 16). Hence we assume that the scalar field with $\mu = 0.01$ is effectively massless in our situation. In this section, we discuss the relation between the QN modes and the horizon area quantization for the Kerr-AdS₅ black holes.

Let us briefly review the Hod's conjecture and its physical interpretation. Hod proposed that the overtone number n may be interpreted as a quantum number characterizing the energy levels of a black hole as an analogy of a hydrogen atom, as in the Bohr's corresponding principle. Based on this idea, the discretized values of the real part of QN frequencies might be associated with the energy of quanta which the black hole can emit or absorb. From this point of view, the mass of a Schwarzschild black hole may be quantized as

$$\Delta M = \lim_{n \rightarrow \infty} \text{Re}(\omega_{lm_1m_2n}), \quad (35)$$

which leads to the horizon area quantization as $\Delta A/4G = \Delta M/T_H$. At least, for the Schwarzschild [35] and Kerr [36,37] black holes, the asymptotic value of the real part of QN frequencies is independent of the angular

³Note that in the ultraspinning limit ($a_1 \rightarrow 1$), the Heun's differential equation in (14) becomes confluent as $u_0 \rightarrow 1$ in the limit. It results in an irregular singular point and the connection problem between irregular and regular singular points is more complicated. Our computation does work at least up to $a_1 = 1 - 10^{-5}$ as demonstrated in Figs. 14 and 15.

⁴We set $\mu = 0.01$ since the calculation of a scattering coefficient $D_1(\omega)$ in (34), whose plots are shown in Figs. 3 and 7, involves the estimation of R_{Div} that is not defined in *Mathematica* when $\Delta = 4$ (i.e., $\mu = 0$).

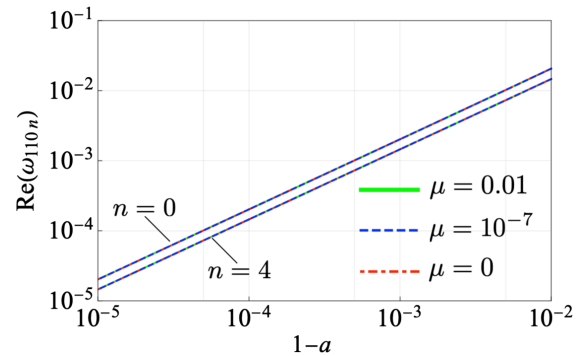


FIG. 16. Real part of QN frequencies of $(l, m_1, m_2) = (1, 1, 0)$ and $n = 0$ and 4. The mass of the scalar field is set to $\mu = 0.01$, 10^{-7} , and 0. The parameters are set to $M = 10$ and $a_1 = a_2$.

index l and is universal. The quantization of the Kerr-AdS₅ black hole mass may also lead to the horizon area quantization.⁵ The first law of black hole thermodynamics in the Kerr-AdS₅ spacetime is [32]

$$\Delta \mathcal{M} = T_H \frac{\Delta A}{4G} + \sum_{i=1}^2 \Omega_i \Delta J_i. \quad (36)$$

Assuming (35), $\Delta J_i = m_i$, and

$$\lim_{n \rightarrow \infty} \text{Re}(\omega_{lm_1m_2n}) \rightarrow \Omega = \sum_i m_i \Omega_i, \quad (37)$$

the first law reduces to

$$T_H \frac{\Delta A}{4G} = 0. \quad (38)$$

It means that when $T_H \neq 0$, the horizon is no longer quantized and becomes a continuum, at least based on the Hod's conjecture. Note that our numerical results just imply that the real part of QN frequencies for the first several overtones approaches Ω , in the low-temperature limit. Therefore, the strong convergence of $\text{Re}(\omega_{lm_1m_2n})$ to Ω for $n \rightarrow \infty$ is still nontrivial from our investigation. Also, for small black holes $\mathcal{M} \ll 1$, the lowest Hawking temperature is zero, and so it is nontrivial if $\Delta A = 0$ at $T_H = 0$. On the other hand, for large black holes, the temperature is nonzero and finite even at the ultraspinning limit, and therefore, the assumption of (37) leads to $\Delta A = 0$ for $\mathcal{M} \gtrsim 1$.

We can show that in the ultraspinning limit, the horizon area of the Kerr-AdS₅ black hole becomes singular. To demonstrate this, let us perform the following coordinate transformations in the metric (1):

⁵However, the Hod's conjecture may be subtle for the Kerr spacetime if the asymptotic value of the real part of QN frequencies is $m\Omega$ for a Kerr black hole with ($a > 0$). The naive application of the Hod's conjecture to that case leads to $\Delta A = 0$. See Refs. [36,37] for more details.

$$\phi \rightarrow \sqrt{1 - a_1^2} \phi, \quad \psi \rightarrow \sqrt{1 - a_2^2} \psi. \quad (39)$$

Considering the geometry of constant (t, r) surface in the near-horizon limit ($r \rightarrow r_+$), the line element for the ultraspinning limit reduces to

$$ds^2 = \lim_{a \rightarrow 1} \frac{r_+^2 + 1}{1 - a^2} \left[d\theta^2 + \frac{(r_+^2 + 1)}{r_+^2} (\sin^2 \theta d\phi + \cos^2 \theta d\psi)^2 \right], \quad (40)$$

where we take $a_1 = a_2 = a$. This shows that in the limit, the horizon area diverges in the coordinates. On the other hand, when we take the limit of $a_1 \rightarrow 1$ while keeping $a_2 < 1$, the topology of the horizon becomes noncompact. As a simple example, let us look into the case of $a_1 \rightarrow 1$ and $a_2 = 0$. In that case, the metric reduces to

$$ds^2 = \frac{(r_+^2 + 1)^2}{\rho^2} \sin^4 \theta d\phi^2 + \frac{r_+^4}{\rho^2} \sin^2 \theta \cos^2 \theta d\psi^2 + \frac{r_+^2 (r_+^2 + 1)}{\rho^2} \cos^4 \theta d\psi^2 + \frac{\rho^2}{\sin^2 \theta} d\theta^2, \quad (41)$$

where we performed the following transformations for the original metric

$$\phi \rightarrow (1 - a_1^2) \phi, \quad \psi \rightarrow (1 - a_2^2) \psi. \quad (42)$$

The metric in (41) appears to be ill-defined at $\theta = 0$. However, by performing a further transformation of

$$\xi = 1 - \cos \theta, \quad (43)$$

the metric near the pole of $\theta = 0$ is

$$ds^2 \simeq (r_+^2 + 1) \left(4\xi^2 d\phi^2 + \frac{d\xi^2}{4\xi^2} \right) + r_+^2 d\psi^2, \quad (44)$$

which has the submanifold of \mathbb{H}^2 on $\phi - \xi$ surface, and we find that the constant (t, r) surface is noncompact in the ultraspinning limit. One can easily find that for $a_1 \rightarrow 1$ and $a_2 \neq 0$, the $\phi - \xi$ surface near $r = r_+$ and $\theta = 0$ is also noncompact as its metric is

$$ds^2 \simeq (r_+^2 + 1) \left(4\xi^2 \frac{r_+^2 + a_2^2}{r_+^2} d\phi^2 + \frac{1}{1 - a_2^2} \frac{d\xi^2}{4\xi^2} \right). \quad (45)$$

Indeed, a similar noncompact horizon appears even in the Kerr-AdS₄ black hole [38–40].

In summary, we have applied the Hod's proposal to our result that the real part of scalar QN frequencies approaches the superradiant frequency in the low-temperature or ultraspinning limits. Then we have concluded that it leads to a continuous horizon area, i.e., unquantized horizon area,

when naively applying the Hod's conjecture to Kerr-AdS₅ black holes. Also, in the special cases involving the ultra-spinning regime, the total horizon area diverges, or the topology of the Kerr-AdS₅ black hole horizon is noncompact.

VI. DISCUSSION AND CONCLUSION

In this paper, we have numerically investigated the structure of scalar quasinormal (QN) frequencies of the five-dimensional Kerr anti-de Sitter (Kerr-AdS₅) black hole. Our numerical investigation covers a broad range of parameter regions for the Kerr-AdS₅ black hole.

In Sec. III A, we have studied the instability of small Kerr-AdS₅ black holes with equal spins. We have confirmed that the strong instability is caused by $l = 1$, and the most unstable QN mode has its frequency close to the superradiant frequency defined by $\Omega \equiv m_1 \Omega_{+,1} + m_2 \Omega_{+,2}$. This is the case even for unequal spins, as shown in Sec. IV A. We have also investigated if the superradiant instability is amplified when the Kerr-AdS₅ black hole has a hierarchy between the two spins, i.e., $a_2/a_1 < 1$. As we have checked that the most unstable harmonics is $(l, m_1, m_2) = (1, 1, 0)$ for $a_2 < a_1$ (Fig. 10), we computed the unstable QN frequencies of $(1, 1, 0)$ mode for different spin ratios while fixing the angular velocity Ω_1 which is equivalent to the superradiant frequency for $(1, 1, 0)$ mode. Then, we have found that the stronger the hierarchy of the two spins is, the more enhanced the instability is (Fig. 11). We conclude that the superradiant instability of the Kerr-AdS₅ black holes is enhanced when the symmetry of the spacetime is reduced. The QN modes that could induce the instability of small Kerr-AdS₅ black holes localize near the real axis in the complex frequency plane. We call those modes type-I modes. On the other hand, we have investigated highly damped QN modes (type-II modes), which differ from the type-I modes and might be relevant to the thermodynamic nature of the Kerr-AdS₅ black hole as the separation of their imaginary part is $\sim 2\pi T_H$. We confirmed that the separation matches $2\pi T_H$ in high accuracy in the low-temperature limit.

In Secs. III B and IV B, we have investigated the scalar QN modes for large Kerr-AdS₅ black holes with equal and unequal spins, respectively. As spin parameters approach the AdS curvature radius, that is the ultraspinning limit ($a_i \rightarrow 1$), type-I modes are suppressed and type-II modes are excited along $\text{Re}(\omega) = \Omega$. The type-II modes with higher damping rates have the periodic separation in their imaginary parts, and the separation for the first several tones matches the surface gravity of the horizon when $a_i \rightarrow 1$ and $\mu \ll 1$ (see Fig. 8). The thermal nature holds even for large Kerr-AdS₅ black holes with unequal spins (Figs. 14 and 15). It would be interesting to study how this property can be relevant to the pole structure of the thermal Green's function in the corresponding conformal field theory (CFT) on the AdS boundary.

TABLE I. The fundamental QN frequency ($n = 0$) and corresponding eigenvalue with $(l, m_1, m_2) = (2, 1, 1)$. The other parameters are set to $M = 0.01$, $a_1 = 10^{-4}$, $a_2 = 9 \times 10^{-5}$, and $\mu = 0.01$. The QN frequency and eigenvalue are shown with high (1st row), medium (2nd row), and low (3rd row) accuracy. The third and fourth columns show the absolute values of the Wronskians for radial and angular modes, respectively.

$\omega_{lm_1m_2n}$	$\lambda_{lm_1m_2n}$	$ W[R_{\text{in}}, R_{\text{AdS}}] $	$ W[S_0, S_{u_0}] $
$5.95740231004969 - 6.71003266747062 \times 10^{-5}i$	$7.99773639983388 + 2.54908885457260 \times 10^{-8}i$	3.5×10^{-13}	1.7×10^{-6}
$5.95740231004 - 6.71003266747 \times 10^{-5}i$	$7.99773639983 + 2.54908885457 \times 10^{-8}i$	7.3×10^{-10}	1.3×10^{-3}
$5.95740231 - 6.71003266 \times 10^{-5}i$	$7.99773639 + 2.54908885 \times 10^{-8}i$	1.3×10^{-7}	3.5

Based on the Hod's conjecture regarding the horizon area quantization [17], the asymptotic value of $\text{Re}(\omega_{lm_1m_2n})$ plays an important role in determining the *one-bit size* of a black hole area ΔA as $T_{\text{H}}\Delta A/4G = \lim_{n \rightarrow \infty} \text{Re}(\omega_{lm_1m_2n}) - \Omega$. Therefore, as we discussed in Sec. V, the convergence of the real part of type-II QN frequencies to Ω for large n implies that the horizon area is no longer quantized but is continuous when naively applying the Hod's conjecture to the Kerr-AdS₅ black holes. From our numerical result, the convergence is likely at least for the low-temperature and ultraspinning regimes. We leave the further study of highly damped QN modes in an analytical way for future work. We also analyzed the horizon topology of the Kerr-AdS₅ black hole and found that in general, an ultraspinning Kerr-AdS₅ black hole has its noncompact horizon.

ACKNOWLEDGMENTS

This work was supported in part by the Special Postdoctoral Researcher (SPDR) Program at RIKEN (N. O.), Incentive Research Project at RIKEN (N. O.), Grant-in-Aid for Scientific Research (KAKENHI) project (21K20371) (N. O.), and Japan Society for the Promotion of Science (JSPS) Grant No. 20J22946 (K. U.).

APPENDIX: ACCURACY OF OUR NUMERICAL COMPUTATION

In this Appendix, we demonstrate the convergence of a QN frequency numerically obtained in our *Mathematica*

notebook. To obtain QN frequencies, we search for the zeros of the following Wronskians in the complex-frequency and complex- λ spaces simultaneously⁶:

$$W[S_0, S_{u_0}]|_{(\omega, \lambda) = (\omega_{lm_1m_2n}, \lambda_{lm_1m_2n})} = W[R_{\text{in}}, R_{\text{AdS}}]|_{(\omega, \lambda) = (\omega_{lm_1m_2n}, \lambda_{lm_1m_2n})} = 0, \quad (\text{A1})$$

where the Wronskian, $W[f(x), g(x)]$, is defined as $W[f, g] \equiv fg' - f'g$. We numerically search for the zeros of the two Wronskians by using a *Mathematica*'s function `FindRoot`. One can increase the accuracy by specifying the value of `WorkingPrecision` more than or comparable to 40. The optimal value of `WorkingPrecision` depends on the background parameters and overtone number we want. In Table I, we show the Wronskians for low, medium, and high accuracies of $(\omega_{lm_1m_2n}, \lambda_{lm_1m_2n})$. It can be seen that the Wronskians approach zero as the accuracy is getting higher. Although Table I shows the QN frequency and eigenvalue with up to 15 digits due to the limitation of space, we obtain those values with higher accuracy (more than or comparable to 40 digits) by choosing a larger value of `WorkingPrecision` as an option in `FindRoot`.

⁶For the explicit forms of S_0 , S_{u_0} , R_{in} , and R_{AdS} , see (22), (23), (30), and (31).

-
- [1] G. 't Hooft, *Conf. Proc. C* **930308**, 284 (1993).
 - [2] L. Susskind, L. Thorlacius, and J. Uglum, *Phys. Rev. D* **48**, 3743 (1993).
 - [3] L. Susskind, *J. Math. Phys. (N.Y.)* **36**, 6377 (1995).
 - [4] J. M. Maldacena, *Adv. Theor. Math. Phys.* **2**, 231 (1998).
 - [5] P. Horava and E. Witten, *Nucl. Phys.* **B475**, 94 (1996).
 - [6] N. Arkani-Hamed, S. Dimopoulos, and G. R. Dvali, *Phys. Lett. B* **429**, 263 (1998).
 - [7] L. Randall and R. Sundrum, *Phys. Rev. Lett.* **83**, 4690 (1999).
 - [8] L. Randall and R. Sundrum, *Phys. Rev. Lett.* **83**, 3370 (1999).
 - [9] N. Arkani-Hamed, S. Dimopoulos, G. R. Dvali, and N. Kaloper, *Phys. Rev. Lett.* **84**, 586 (2000).
 - [10] L. Susskind, [arXiv:hep-th/0302219](https://arxiv.org/abs/hep-th/0302219).
 - [11] E. Witten, *Adv. Theor. Math. Phys.* **2**, 253 (1998).
 - [12] T. Banks, M. R. Douglas, G. T. Horowitz, and E. J. Martinec, [arXiv:hep-th/9808016](https://arxiv.org/abs/hep-th/9808016).
 - [13] P. Kraus, *J. High Energy Phys.* **12** (1999) 011.
 - [14] D. Ida, *J. High Energy Phys.* **09** (2000) 014.

- [15] S. Mukohyama, *Phys. Lett. B* **473**, 241 (2000).
- [16] D. Birmingham, I. Sachs, and S. N. Solodukhin, *Phys. Rev. Lett.* **88**, 151301 (2002).
- [17] S. Hod, *Phys. Rev. Lett.* **81**, 4293 (1998).
- [18] R. C. Myers and M. J. Perry, *Ann. Phys. (N.Y.)* **172**, 304 (1986).
- [19] S. W. Hawking, C. J. Hunter, and M. Taylor, *Phys. Rev. D* **59**, 064005 (1999).
- [20] A. N. Aliev and O. Delice, *Phys. Rev. D* **79**, 024013 (2009).
- [21] K. Murata, *Prog. Theor. Phys.* **121**, 1099 (2009).
- [22] K. Murata, T. Nishioka, and N. Tanahashi, *Prog. Theor. Phys.* **121**, 941 (2009).
- [23] V. Cardoso, O. J. C. Dias, G. S. Hartnett, L. Lehner, and J. E. Santos, *J. High Energy Phys.* **04** (2014) 183.
- [24] I. Y. Aref'eva, A. A. Golubtsova, and E. Gourgoulhon, *J. High Energy Phys.* **04** (2021) 169.
- [25] J. Nian and L. A. Pando Zayas, *J. High Energy Phys.* **07** (2020) 120.
- [26] J. Barragán Amado, B. Carneiro Da Cunha, and E. Pallante, *Phys. Rev. D* **99**, 105006 (2019).
- [27] J. B. Amado, B. Carneiro da Cunha, and E. Pallante, *J. High Energy Phys.* **04** (2020) 155.
- [28] J. Barragán Amado, B. Carneiro da Cunha, and E. Pallante, *J. High Energy Phys.* **05** (2021) 251.
- [29] B. C. da Cunha and J. a. P. Cavalcante, *Phys. Rev. D* **104**, 084051 (2021).
- [30] J. B. Amado, B. C. da Cunha, and E. Pallante, *Phys. Rev. D* **105**, 044028 (2022).
- [31] J. B. Amado, B. Carneiro da Cunha, and E. Pallante, *J. High Energy Phys.* **08** (2017) 094.
- [32] G. W. Gibbons, M. J. Perry, and C. N. Pope, *Classical Quantum Gravity* **22**, 1503 (2005).
- [33] S. Hollands, A. Ishibashi, and D. Marolf, *Classical Quantum Gravity* **22**, 2881 (2005).
- [34] R. Olea, *J. High Energy Phys.* **04** (2007) 073.
- [35] L. Motl, *Adv. Theor. Math. Phys.* **6**, 1135 (2002).
- [36] E. Berti, V. Cardoso, K. D. Kokkotas, and H. Onozawa, *Phys. Rev. D* **68**, 124018 (2003).
- [37] E. Berti, V. Cardoso, and S. Yoshida, *Phys. Rev. D* **69**, 124018 (2004).
- [38] D. Klemm, *Phys. Rev. D* **89**, 084007 (2014).
- [39] R. A. Hennigar, D. Kubizňák, and R. B. Mann, *Phys. Rev. Lett.* **115**, 031101 (2015).
- [40] R. A. Hennigar, D. Kubizňák, R. B. Mann, and N. Musoke, *J. High Energy Phys.* **06** (2015) 096.